

A joint model for DHS and MICS surveys: Spatial modeling with anonymized locations

John Paige^{a,*}, Geir-Arne Fuglstad^a, Andrea Riebler^a

^a*Department of Mathematical Sciences, NTNU, Trondheim, Norway*

Abstract

Anonymizing the GPS locations of observations can bias a spatial model's parameter estimates and attenuate spatial predictions when improperly accounted for, and is relevant in applications from public health to paleoseismology. In this work, we demonstrate that a newly introduced method for geostatistical modeling in the presence of anonymized point locations can be extended to account for more general kinds of positional uncertainty due to location anonymization, including both jittering (a form of random perturbations of GPS coordinates) and geomasking (reporting only the name of the area containing the true GPS coordinates). We further provide a numerical integration scheme that flexibly accounts for the positional uncertainty as well as spatial and covariate information.

We apply the method to women's secondary education completion data in the 2018 Nigeria demographic and health survey (NDHS) containing jittered point locations, and the 2016 Nigeria multiple indicator cluster survey (NMICS) containing geomasked locations. We show that accounting for the positional uncertainty in the surveys can improve predictions in terms of their continuous rank probability score.

Keywords: Small area estimation; Location anonymization; Positional uncertainty; Geomasking; Jittering.

2020 MSC: 62H11, 62P99

*Corresponding author

Email address: john.paige@ntnu.no (John Paige)

1. Introduction

Geostatistical modeling of health and demographic indicators at fine spatial scales is increasingly emphasized ([LBD Child Growth Failure Collaborators and others, 2020](#); [Osgood-Zimmerman et al., 2018](#)). This is true for a number of reasons, including the improved ability to target populations that most need assistance when aiming to reach various UN sustainable development goals (SDGs), which set targets for a number of health and demographic indicators to reach by 2030 ([United Nations, 2020](#)). These SDGs explicitly state the importance of reducing inequality in health and demographic outcomes both demographically and spatially.

Since official statistics in low and middle income countries frequently exhibit substantial bias, third party surveys are typically considered the gold standard for data in such contexts ([Li et al., 2019](#); [Wagner et al., 2018](#); [Sandefur and Glassman, 2015](#); [Jerven, 2013](#); [Devarajan, 2013](#)). Demographic and health surveys (DHS, [USAID, 2024](#)) and multiple indicator cluster surveys (MICS, [IPUMS, 2024](#)) are two kinds of surveys that are frequently used for estimating health and demographic indicators in low and middle income countries ([LBD Child Growth Failure Collaborators and others, 2020](#); [Osgood-Zimmerman et al., 2018](#); [Paige et al., 2022c](#); [Burstein et al., 2018](#); [Godwin and Wakefield, 2021](#); [Graetz et al., 2018](#)).

Yet using DHS and MICS surveys to produce predictions at fine spatial or temporal scales can be challenging for two reasons we hope to address in this work. First, DHS and MICS surveys deliberately adjust the spatial locations of the surveyed clusters (i.e. surveyed villages and city neighborhoods) for anonymity purposes ([ICF International, 2012](#)), resulting in uncertainty in the clusters' spatial locations known as positional uncertainty. This positional uncertainty is routinely ignored in classical and commonly used geostatistical models. Yet ignoring location anonymization in geostatistical models, has been shown to lead to attenuated parameter estimates, and can reduce estimated

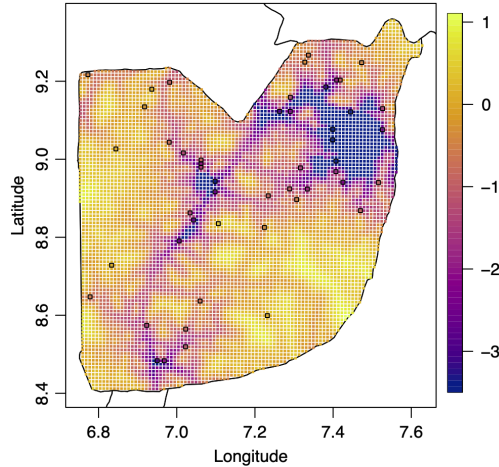


Figure 1: Illustration of positional uncertainty in FCT Abuja, Nigeria. Black points represent example locations of an observation, and colors indicate the value of a transformed covariate, healthcare inaccessibility.

spatial dependency along with predictive ability (Cressie and Kornak, 2003; Fanshawe and Diggle, 2011; Fronterre et al., 2018).

Figure 1 illustrates how the positional uncertainty of a single cluster might affect its response if it could be anywhere within the Federal Capital Territory (FCT) Abuja in Nigeria. Depending on the location of the cluster, the effect of the depicted covariate could vary substantially, influencing predictions for that cluster. The black points in the figure are technically integration points generated based on the numerical integration scheme described in Section 3, but can be thought of as a set of example locations that a single cluster might have.

Second, while DHS and MICS surveys can help in these contexts, they are costly and sparse (Paige et al., 2022b; Marquez and Wakefield, 2021), and finer and finer scale estimation of health and demographic indicators necessitates more and more data. DHS and MICS surveys use two different kinds of anonymization, and hence exhibit two different kinds of positional uncertainty, but a framework has not yet been developed to jointly model responses from the surveys while accounting for their different forms of location anonymization

in a principled way.

While it is common to assume point locations of the modeled observations are known, some methods can account for uncertainty in the point locations in certain contexts. For example, [Cressie and Kornak \(2003\)](#) propose a way to perform kriging in the presence of positional uncertainty by adjusting the covariates and the covariance function, using a pseudolikelihood approach for parameter estimation. Their approach assumes a linear model, however, and a Berkson type error model ([Carroll et al., 2006](#)) for the locations, which is not suitable for this context. [Fanshawe and Diggle \(2011\)](#) propose a general method for accounting for positional uncertainty using a combination of Monte Carlo likelihood maximization for inference and numerical integration for prediction. They note that likelihood maximization took 72 hours for modeling data at 148 spatial locations, however. [Wilson and Wakefield \(2021\)](#) proposed using integrated nested Laplace approximations within Markov chain Monte Carlo (MCMC, [Gómez-Rubio and Rue, 2018](#)) to handle general forms of point location anonymization and the resulting positional uncertainty within Bayesian hierarchical models with a spatial random effect, but they note that the method took 52 hours to generate 1000 MCMC samples.

More recently, [Altay et al. \(2022\)](#) proposed a numerical integration method for fitting spatial Bayesian hierarchical models under jittering. They showed that the method could be used to speed up inference considerably compared to [Fanshawe and Diggle \(2011\)](#) and [Wilson and Wakefield \(2021\)](#). [Altay et al. \(2024\)](#) further demonstrated that the model could be used effectively in the presence of raster based covariates, and that jittering could, if not handled properly, attenuate raster based covariate effect size estimates.

In this paper, we extend the method proposed in [Altay et al. \(2022\)](#) to account for more general forms of positional anonymization, and where the resulting positional uncertainty is potentially much larger than in DHS surveys. As a result, our proposed method is able to jointly model DHS and MICS data, and it can do so at a fraction of the time of existing approaches that can be applied in such contexts. Moreover, it can account for the positional uncertainty

present in DHS and MICS data under a principled statistical framework.

In Section 2 we discuss the details of the data we use in our analysis, including the DHS and MICS surveys. In Section 3 we introduce a classical geostatistical model for health and demographic indicators, and show how it can be modified to create a joint spatial model accounting for anonymization of spatial positions in DHS and MICS surveys jointly. In Section 4 we perform a validation of the proposed model along with several others for comparison. In Section 5, we apply some of the considered models to the chosen application, which involved estimating women’s secondary education prevalence in Nigeria. Finally, we summarize our conclusions in Section 6.

2. Data

2.1. Household survey data

Both the 2018 Nigeria demographic and health survey (NDHS) ([National Population Commission \(NPC\) \[Nigeria\] and ICF, 2019](#)) and the 2016 Nigeria multiple indicator cluster survey (NMICS) ([Nigeria National Bureau of Statistics, 2016](#)) sample enumeration areas (EAs), villages and city neighborhoods defined by the 2006 Population Census. EAs are defined by the census, and are officially defined as either urban or rural. The NDHS selects a fixed number of EAs from the urban and rural parts of each of the 37 Admin1 areas (states), the administrative districts below the national level, and the EAs are selected with probability proportional to size (PPS) sampling. In the 2018 NMICS, a fixed number of EAs are selected from 35 Admin1 areas and the three senatorial districts in each the Kano and Lagos states. Hence, the NDHS is stratified with strata equal to the urban/rural parts of each Admin1 area, making 74 strata, whereas the NMICS strata are 35 Admin1 areas and 6 senatorial districts, making 41 strata in total. The NDHS samples 25 households from each selected EA to be included in the survey, whereas the NMICS samples 16 households from each selected EA. Both use simple random sampling for sampling households within selected EAs to form the sampled clusters. In total, the NDHS

and NMICS have 1,379 and 2,195 clusters and 13,980 and 11,037 women aged 20–29 respectively.

Response rates for both surveys were high, particularly for the NDHS, with women’s response rates being 94% for the NMICS and 99% for the NDHS. We consider women without any formal education to have not completed their secondary education, in part because literacy rates are lower among women without a formal education than women who have only attended primary school.

For privacy reasons both the DHS and MICS often anonymize the cluster centroid point locations in two different ways. In DHS surveys, it is common to *jitter* cluster locations, which involves displacing them by uniformly distributed random angles and radii (ICF International, 2012; Burgert et al., 2013). NDHS cluster centroids in urban areas are jittered by up to 2 km, and 99% of rural locations are jittered by up to 5 km with 1% of them being jittered by up to 10 km. In MICS surveys, cluster locations are *geomasked*, which means that only the administrative area containing the cluster GPS coordinates along with the clusters urban/rural level is known (Khan and Hancioglu, 2019; National Bureau of Statistics (NBS) and United Nations Children’s Fund (UNICEF), 2017). The locations of the NMICS clusters therefore typically have much more positional uncertainty than the NDHS cluster locations. Such levels of positional uncertainty make it difficult for fine scale geostatistical models to incorporate MICS data.

The responses of both surveys are plotted spatially in Figure 2, where individual responses from the MICS survey are naively averaged (all individual respondents are weighted equally) at the MICS stratum level to produce the areal averages depicted. The depicted DHS responses are averaged across individual responses with equal weight for each cluster, and are plotted at the jittered (observed) cluster locations rather than the unknown true locations.

2.2. Covariate rasters

We consider five different raster-based covariates: population density as estimated by WorldPop (World Pop, 2022), urban/rural classifications we generate

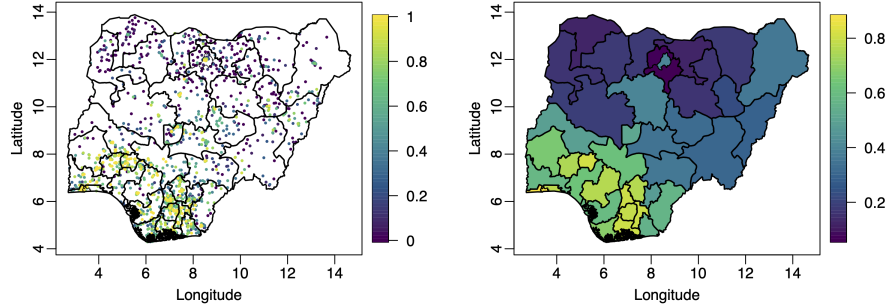


Figure 2: Women’s secondary education prevalence from DHS (left) and MICS (right) surveys. Admin1 areas and 6 senatorial districts are outlined in thick and thin lines respectively.

based on population density, access to healthcare as measured in travel time (Weiss et al., 2018), elevation (NOAA, 2022), and distance to rivers and lakes (Natural Earth, 2012). We transform most of these covariates and then normalize them, subtracting the mean and dividing by the standard deviation. The transformation and renormalization of the covariate rasters is intended to improve the interpretability of the relative effect sizes and the accuracy of the numerical integration. After calibrating population density within each admin2 area to be proportional to the estimated total urban and rural populations, the resulting population density raster is transformed via the $\log(x + 1)$ function. The healthcare inaccessibility variable is also $\log(x + 1)$ -transformed, whereas elevation is square root transformed, and distance to rivers and lakes is not transformed prior to normalization. Urbanicity classification is neither transformed nor normalized, since it is a binary variable. Urbanicity classifications are generated based on thresholding untransformed population density surface so as to ensure urban and rural populations are as close to the estimated numbers as possible, with any deviations removed through calibration as per Paige et al. (2022b) and Paige et al. (2022c).

3. Methods

3.1. Spatial risk model

We let $r(t)$ be the typical spatial probability (risk) of a woman aged 20–29 completing her secondary education at location $t \in \mathcal{D}$, with $\mathcal{D} \subset \mathbb{R}^2$ representing the spatial domain, Nigeria. This risk is then modeled as:

$$\text{logit}(r(t)) = \mathbf{d}(t)^T \boldsymbol{\beta} + u(t). \quad (1)$$

The intercept and spatial fixed effects are given by $\mathbf{d}(t)^T \boldsymbol{\beta}$. We model the spatial random effects, $u(t)$, using a reparameterization of the Besag-York-Mollie (BYM) model referred to as BYM2 (Riebler et al., 2016), and it can be represented as,

$$u(t) = \frac{1}{\sqrt{\tau}} \left(\sqrt{\phi} \mathbf{w}_{A[t]} + \sqrt{1 - \phi} \mathbf{v}_{A[t]} \right),$$

where \mathbf{w} represents spatially structured random effects, and \mathbf{v} represents iid unstructured random effects. Both \mathbf{w} and \mathbf{v} have mean zero and unit generalized variance, and $A[t]$ gives the index of the modeled area associated with location t . The generalized precision of u is given by τ , and ϕ is the proportion of variance that is structured.

We assume that $A[t]$ is the MICS stratum associated with t so that the BYM2 effect varies at the level of the geomasked area (hence, it varies at the Admin1 level except in Lagos and Kano, where it is modeled at the senatorial district level).

3.2. Response model

We model the responses for a given survey, whether it be DHS or MICS. Let y_c , $c = 1, \dots, C$ be the number of women aged 20–29 who completed their secondary education at cluster c for that survey, which contains C clusters. We assume $t_c \in \mathcal{D}$ for $c = 1, \dots, C$ are the true locations of the clusters in the

survey. The response model is then:

$$\begin{aligned}
y_c \mid r^{\text{clust}}(t_c) &\sim \text{Bin}(n_c, r^{\text{clust}}(t_c)), \\
\text{logit}(r^{\text{clust}}(t_c)) &= \text{logit}(r(t_c)) + \epsilon_c \\
&= \mathbf{d}(t_c)^T \boldsymbol{\beta} + u(t_c) + \epsilon_c, \quad c = 1, \dots, C. \quad (2)
\end{aligned}$$

Here, $r^{\text{clust}}(t_c)$ is the risk for women specifically in cluster c , which is the same as $r(t_c)$ except it contains an additional cluster level random intercept, ϵ_c , representing the influence of cluster specific conditions on the risk. The ϵ_c for $c = 1, \dots, C$ are independent and identically distributed (iid) zero mean Gaussian noise with variance given by σ_ϵ^2 . In addition, n_c is the known number of women aged 20–29 in cluster c .

We assume the spatial risk model (1) as well as the response model (2) apply to both the DHS and MICS surveys. Conditional on the risk, the responses are assumed to be independent across clusters as well as surveys.

Throughout this work we use penalized complexity (PC) priors (Simpson et al., 2017), which allow for a general framework for penalizing random effects, shrinking models towards a base model without random effects or with simplified structure in available random effects. We place a PC prior on the BYM2 precision and nugget standard deviation parameters so that $P(1/\sqrt{\tau} < 1) = P(\sigma_\epsilon < 1) = 0.1$, and a PC prior on the BYM2 proportion of structured variance, ϕ , so that $P(\phi < 0.5) = 2/3$ as recommended in Riebler et al. (2016).

3.3. Accounting for positional uncertainty in DHS and MICS surveys

3.3.1. Distributional forms of positional anonymization

We assume that a cluster c in survey j may have true location $t_c^j \in \mathcal{D}$ for $j \in \{\text{DHS}, \text{MICS}\}$ and observed location $s_c^{\text{DHS}} \in \mathcal{D}$ in the case of DHS data or $s_c^{\text{MICS}} \subset \mathcal{D}$ in the case of MICS data. Note that s_c^j is a point location for $j = \text{DHS}$ and an area for $j = \text{MICS}$. The DHS cluster locations are jittered within a relatively short distance of the respective true locations. DHS cluster locations are jittered in a uniform distributed random direction from 0 to 2π ,

and by a uniform distributed radius from 0 to the maximum jittering distance.

The jittering distribution of the observed urban DHS location s_c^{DHS} is:

$$\pi(s_c^{\text{DHS}} | t_c^{\text{DHS}}) \propto \frac{\mathbb{I}\{A_2[s_c^{\text{DHS}}] = A_2[t_c^{\text{DHS}}]\} \cdot \mathbb{I}\{|s_c^{\text{DHS}} - t_c^{\text{DHS}}| < 2\}}{|s_c^{\text{DHS}} - t_c^{\text{DHS}}|}, \quad \text{urb}^{\text{DHS}}[c] = \text{urban},$$

where coordinates are easting/northing in kilometers, $\mathbb{I}\{\cdot\}$ is an indicator function, and $\text{urb}^j[c]$ is the known urban/rural level of cluster c in survey j . Here, $A_2[t]$ is the Admin2 area associated with location t . Note that, generally, DHS cluster locations are never jittered outside of Admin1 boundaries for surveys before 2008, or Admin2 boundaries for DHS surveys after 2008 (Perez-Heydrich et al., 2013). Hence, for DHS surveys taken before 2008, the $A_2[t]$ term should be changed from an Admin2 to an Admin1 level term.

Since 99% of rural clusters are jittered up to 5 km, with 1% of rural clusters are jittered up to 10 km, rural DHS cluster locations have the following jittering distribution:

$$\pi(s_c^{\text{DHS}} | t_c^{\text{DHS}}) \propto \frac{\mathbb{I}\{A_2[s_c^{\text{DHS}}] = A_2[t_c^{\text{DHS}}]\}}{|s_c^{\text{DHS}} - t_c^{\text{DHS}}|} \left[\frac{99 \cdot \mathbb{I}\{|s_c^{\text{DHS}} - t_c^{\text{DHS}}| < 5\}}{100} + \frac{\mathbb{I}\{|s_c^{\text{DHS}} - t_c^{\text{DHS}}| < 10\}}{100} \right], \quad \text{urb}^{\text{DHS}}[c] = \text{rural}.$$

MICS cluster point locations are known only up to the MICS stratum they lie in and their urban/rural level. Hence, the distribution for the MICS cluster positions given the true locations is much simpler, with $\pi(s_c^{\text{MICS}} | t_c^{\text{DHS}}) = \mathbb{I}\{s_c^{\text{MICS}} \ni t_c^{\text{MICS}}\}$, where ‘ \ni ’ denotes ‘contains’, and recalling that s_c^{MICS} is the geomasked area for cluster c of the MICS survey.

3.3.2. Likelihoods under positional uncertainty

We extend the model proposed in Altay et al. (2022) and Altay et al. (2024) by generalizing it to account for geomasking in a joint model for DHS and MICS surveys. For a given survey we write the likelihood conditional on the underlying risk as:

$$\begin{aligned} \pi(y_c, s_c | r(\cdot)) &= \int_{\mathcal{D}} \pi(y_c, s_c | r(t_c)) \pi(t_c) dt_c, \\ &= \int_{\mathcal{D}} \pi(y_c | r(t_c)) \pi(s_c | t_c) \pi(t_c) dt_c, \end{aligned} \quad (3)$$

for $c = 1, \dots, C$. Again, we assume the cluster level responses are conditionally independent given the underlying risk, both within and between surveys.

We assume that, *a priori*, the distribution of true cluster locations is proportional to population density, since the EAs forming the clusters are constructed in the census to have roughly equal populations. Hence, for both DHS and MICS surveys, we assume that $\pi(t_c) \propto q(t_c)$ for each cluster $c = 1, \dots, C$ in a given survey, where $q(\cdot)$ is the population density as a function of spatial location as calculated from the WorldPop data described in Section 2.2.

Note that while the official urbanicity level of all clusters in both the DHS and MICS surveys is known, the official urbanicity designation at any given spatial location is unknown. We must therefore classify urbanicity spatially ourselves as discussed in Section 2.2, and as demonstrated in (Paige et al., 2022b). In order to ensure consistency between inference and spatial prediction, we constrain the support of the prior over true cluster locations, $\pi(t_c)$, to be have the correct urbanicity level for MICS clusters, i.e. to have support $\{t \in A[t_c] : \text{urbanicity}(t) = \text{urb}^{\text{MICS}}[c]\}$, where $\text{urbanicity}(t)$ is the urbanicity classification raster generated as described in Section 2.2, and where $A[t]$ is the MICS stratum containing cluster location $t \in \mathcal{D}$. We opt against restricting the support of the priors for the DHS cluster locations based on urbanicity, since the DHS cluster locations are known to a much higher degree of accuracy, and also are sometimes not close enough to the nearest pixel classified with a matching urbanicity level. In both cases, the urbanicity covariate used in the response model for a given cluster is its true known urbanicity, while the classified urbanicity raster is used in pixel level and aggregated predictions.

3.3.3. Implementation and computation

For each cluster c in the given survey, we evaluate (3) numerically via,

$$\pi(y_c, s_c | r(\cdot)) \approx \sum_{k=1}^K \alpha_{ck} \pi(y_c | r(\tilde{t}_{ck})) \pi(s_c | \tilde{t}_{ck}) \pi(\tilde{t}_{ck}), \quad (4)$$

for integration weights α_{ck} and associated with integration points \tilde{t}_{ck} , for $k = 1, \dots, K$, where integration points and weights are as given in Altay et al. (2022)

for DHS clusters. The weights and integration points associated with a given MICS cluster c are given in the supplementary material in Section S.1. For both both the DHS and MICS integration schemes, we take $\omega_{ck} \propto \alpha_{ck} \pi(s_c | \tilde{f}_{ck}) \pi(\tilde{f}_{ck})$, and require $\sum_k \omega_{ck} = 1$ for each fixed cluster c . We can renormalize in this way provided the renormalization constants are functions of fixed quantities, and in this case they are only a function of quantities fixed prior to the analysis: population density, the covariate rasters, and the number of integration points. The resulting numerical integral for the likelihood is then calculated as:

$$\pi(y_c, s_c | r(\cdot)) \dot{\propto} \sum_{k=1}^K \omega_{ck} \pi(y_c | r(\tilde{f}_{ck})),$$

where $\dot{\propto}$ denotes ‘approximately proportional to’, and the constant of proportionality depends only on quantities fixed prior to the analysis.

We choose integration points in a very different way for MICS clusters than for DHS clusters. Since covariates vary over the support of the more diffuse distributions of cluster positions, we choose integration points that can better represent the full range of possible combinations of covariate values. Since the integration points and weights are calculated only once, it is possible to choose them carefully without spending much computational effort overall. More information on choosing the integration points and weights, along with illustrations, is given in the Supplement in Section S.1. We choose K to be 100 for MICS clusters, 11 for urban DHS clusters, and 16 for rural DHS clusters in order to achieve a good blend of computational speed and accuracy.

4. Model validation

4.1. Validation overview and compared approaches

In order to evaluate the considered approaches, we perform two kinds of validation: validation of Admin1 level areal predictions, and validation of left out clusters. We wished to validate both at the cluster and areal levels in part to simply explore a new possible way to validate individual cluster level predictions with unknown spatial locations, which has potential applications in validating

aggregation models (Paige et al., 2022c), and in part due to the fact that areal and cluster level prediction may ultimately have different needs. We discuss this in greater detail later in this section, and in Section 6.

We consider 4 approaches in order of increasing complexity denoted by M_d , M_D , M_{Dm} , and M_{DM} depending on whether the MCIS data is included, and whether positional uncertainty in the DHS and MICS datasets is fully accounted for:

M_d : Only DHS data is included, and the observed locations are assumed to be the true locations.

M_D : Only DHS data is included, and jittering is accounted for using the proposed method.

M_{dm} : Both DHS and MICS data is included, and position error is not accounted for in either dataset. For each MICS cluster a single location is randomly drawn from within its MICS stratum with probability proportional to population density. This randomly drawn location is assumed to be the true location of the corresponding MICS cluster.

M_{DM} : Both DHS and MICS data is included, and positional uncertainty is accounted for in both datasets using the proposed method.

Note that the method for simulating MICS cluster locations in the M_{dm} approach is the same as in (LBD Child Growth Failure Collaborators and others, 2020). As in (LBD Child Growth Failure Collaborators and others, 2020), the M_{dm} approach does not account for positional uncertainty in either the DHS or the MICS datasets.

When validating against left out individual clusters, we perform a stratified 20-fold validation, with 10 folds consisting entirely of DHS data, and 10 consisting of MICS data. For DHS survey data, validation folds are stratified by Admin1 areas and urbanicity, whereas for the MICS survey, validation folds are

stratified by the 41 MICS stratum areas and urbanicity. We ensure that the number of clusters in any one stratum differs by at most 1 across all 10 folds for a given survey. Since the M_{dm} and M_{DM} approaches depend on data from both surveys, they must each be fit 20 times to generate 20 sets of predictions each. Since the M_d and M_D approaches only use the DHS data, we fit them and generate predictions 11 times—10 times for each fold of the DHS data left out, and one additional time using all of the DHS data, since leaving out different MICS folds results in the same model under those two approaches.

In the case where we validate areal predictions, we leave out 10 of the above 20 folds in a single area at a time—five (randomly selected) folds from each survey. We then produce Admin1 level survey-weighted direct estimators using the `svyglm` function from the `survey` package (Lumley, 2023), with a Horvitz-Thompson type variance estimate (Horvitz and Thompson, 1952) based on the left out DHS data, the left out MICS data, and a precision-weighted average of the two. Here, `svyglm` produces an estimator by solving the classical set of survey-weighted score equations for fitting generalized linear models to survey data (see, e.g. Binder 1983; Lumley and Scott 2017). Finally, we compare each approach’s Admin1 level predictions against the direct estimate as recommended in (DHS, 2021).

Note that since the direct estimate, unlike the model based estimate, includes sampling variability, it is necessary to add such sampling variability into the model based estimate so that the prediction represents a prediction for the left out data rather than for the entire population in the area. To do so, we follow a procedure equivalent to that of Gascoigne et al. (2023), except that the final validation scores and metrics are all calculated on a probability scale.

Letting Y_i be the left out direct estimate for the prevalence of women’s secondary education completion in area $i = 1, \dots, 37$, and \hat{Y}_i be the model based estimate, we consider the difference $\hat{Y}_i - Y_i$, which should generally be closer to zero the better at model is a producing areal estimates. Since \hat{Y}_i and Y_i are produced from different data sources, they are independent estimators. This means that if one were to sample M independent replicates from their sampling distributions,

$Y_i^{(1)}, \dots, Y_i^{(M)}$ from the asymptotic distribution of Y_i , and $\hat{Y}_i^{(1)}, \dots, \hat{Y}_i^{(M)}$ from the posterior distribution of \hat{Y}_i , then $\hat{Y}_i^{(1)} - Y_i^{(1)}, \dots, \hat{Y}_i^{(M)} - Y_i^{(M)}$, would be M samples from the distribution of $\hat{Y}_i - Y_i$. Using the evaluation metrics in the section below, we can then compare the distribution of $\hat{Y}_i - Y_i$ against 0, the target value. This validation scheme has the advantage that it targets predictions for a population as opposed to targeting spatial predictions. Also, it accounts for the survey weights.

4.2. Evaluation metrics for single predictions

For scoring metrics, we consider mean square error (MSE), continuous rank probability score (CRPS), interval score (IS) for 95% CIs, fuzzy empirical coverage, and 95% fuzzy CI width. Note that CRPS and IS are strictly proper and proper scoring rules respectively, so that the expected value of the scores of true model is strictly or nonstrictly smaller than those of incorrect models (Gneiting and Raftery, 2007). Fuzzy empirical coverage and fuzzy CI width (Paige et al., 2022a) are employed to eliminate artifacts due to discrete confidence/credible intervals and data distributions. They are based on fuzzy intervals (Geyer and Meeden, 2005), and are identical to the typical measure of empirical coverage and CI width in the case of continuous distributions.

Scoring rules and metrics are evaluated for a given target y and predictive distribution P , where y is a prevalence and is therefore on a probability scale:

$$\begin{aligned} \text{MSE}(y; P) &= (y - E_P[y])^2 \\ \text{CRPS}(y; P) &= \int_{-\infty}^{\infty} (P(y \leq \tilde{y}) - \mathbb{I}\{y \leq \tilde{y}\})^2 d\tilde{y} \\ \text{IS}_\alpha(y; P) &= (u - l) + \frac{2}{\alpha}(y - u)\mathbb{I}\{y > u\} + \frac{2}{\alpha}(l - y)\mathbb{I}\{y < l\} \\ \text{Cvg}_\alpha^{\text{fuzzy}}(y; P) &= E_P[\mathbb{I}\{L_\alpha^{\text{fuzzy}} \leq y \leq U_\alpha^{\text{fuzzy}}\}] \\ \text{Width}_\alpha^{\text{fuzzy}}(y; P) &= E_P[U_\alpha^{\text{fuzzy}} - L_\alpha^{\text{fuzzy}}], \end{aligned}$$

where $[l, u]$ is a credible interval for y/n based on predictive distribution P with significance at most α , where $l = \sup\{x : P(x) \leq \alpha/2\}$ and $u = \inf\{x : P(u) < 1 - \alpha/2\}$. Similarly, $[L_\alpha^{\text{fuzzy}}, U_\alpha^{\text{fuzzy}}]$ is a fuzzy credible interval for y based

on predictive distribution P with significance equal to α . Note that l and u in the expression for $\text{IS}_\alpha(y; P)$ are the fixed lower and upper endpoints for the α significance equal tailed credible interval given by predictive distribution P . Fuzzy endpoints L_α^{fuzzy} and U_α^{fuzzy} are not used in the interval score, since they would not result in a proper scoring rule.

4.3. Aggregating evaluation metrics

We first consider cluster level validation. Due to positional uncertainty, we are only able to validate cluster level predictions in the case where the cluster location is unknown. The considered validation task is then to predict the response for a given out of sampled cluster conditional on the observed (with positional uncertainty) location.

Letting $\mathcal{O}_1^j, \dots, \mathcal{O}_{10}^j$ be the sets of indices of the out of sample clusters for the 10 cross validation folds for survey j , and let $\mathcal{I}_1^j, \dots, \mathcal{I}_{10}^j$ be the in sample data as well as other information used for prediction such as the observed locations of the out of sample clusters. Given a score or metric $S(y; P)$ for a single cluster prevalence y and predictive distribution P , we consider the cluster level validation score averaging over each fold k and dataset j as,

$$S_{\text{clust}}^j = \frac{1}{N^j} \sum_{k=1}^{10} \sum_{c \in \mathcal{O}_k^j} n_c^j \cdot S\left(y_c^j; P(\cdot | \mathcal{I}_k^j)\right),$$

where P is the predictive distribution under a given approach for a given set of sample cluster locations and target population sizes. Here, y_c^j and n_c^j are the prevalence and number of individuals in the target population in cluster c and dataset j , and N^j are the number of individuals in dataset j . We also take a weighted average of the scores for each survey,

$$S_{\text{clust}}^{\text{DHS}+\text{MICS}} = \frac{N^{\text{DHS}}}{N^{\text{DHS}} + N^{\text{MICS}}} S_{\text{clust}}^{\text{DHS}} + \frac{N^{\text{MICS}}}{N^{\text{DHS}} + N^{\text{MICS}}} S_{\text{clust}}^{\text{MICS}},$$

as a measure of overall performance across both datasets, where the weights are proportional to the sample sizes.

In the case of areal validation, let \hat{Y}_i be the areal prediction for Admin1 area i , $i = 1, \dots, 37$, and let Y_i^j be the direct estimate for area i and dataset

j , where $j = \text{DHS}, \text{MICS}, \text{DHS}+\text{MICS}$. Here, $j = \text{DHS}+\text{MICS}$ corresponds to the case where model based areal predictions are compared against the precision weighted average of the DHS and MICS direct estimates. We calculate a simple, unweighted average of metrics across areas:

$$S_{\text{areal}}^j = \frac{1}{37} \sum_{i=1}^{37} S\left(0; P_{\hat{Y}_i - Y_i^j}\right),$$

where $P_{\hat{Y}_i - Y_i^j}$ is the distribution of $\hat{Y}_i - Y_i^j$ calculated as described in Section 4.1. Note that we can compare the same model based estimator, \hat{Y}_i , against three different direct estimators, which gives an idea of how well the model based estimator can predict data from each survey separately as well as altogether.

4.4. Validation results

Areal validation scores and metrics are provided in Table 1. A complete set of validation results are given in the Supplement in Tables C.5 and C.6. We focus here on CRPS as a single measure of overall predictive ability, since it is a strictly proper scoring rule, but include other metrics for interpretation purposes.

We find that accounting for positional uncertainty tends to improve model areal predictions in terms of both CRPS and IS. For example, in Table 1 we consistently observed that M_D has better CRPS and IS than M_d , and that M_{DM} has better CRPS and IS than M_{dm} . This is true regardless of the validation data being MICS, DHS, or a combination. We see particular improvement from the M_d model to the M_D model.

Interestingly, adding the MICS data does not seem to lead to improved predictions of DHS data. While the included 2018 DHS and 2016 MICS surveys are both high quality and nearby in time, there are always some fluctuations in population means from year to year. It should therefore not be so surprising that including MICS data lead to worse predictions for left out DHS data in terms of CRPS, both for areal and cluster level validation. Including the MICS data also did not improve predictions for the MICS clusters by so much, however.

Approach	CRPS	IS	Cvg	Width	Time (minutes)
<i>DHS+MICS</i>					
M _d	0.042	0.427	0.89	0.236	0.04
M _D	0.037	0.332	0.89	0.222	1.16
M _{dm}	0.040	0.430	0.81	0.208	0.08
M _{DM}	0.039	0.415	0.81	0.203	13.42
<i>DHS</i>					
M _d	0.045	0.554	0.92	0.280	0.04
M _D	0.040	0.478	0.92	0.268	1.16
M _{dm}	0.047	0.520	0.89	0.255	0.08
M _{DM}	0.046	0.519	0.95	0.251	13.42
<i>MICS</i>					
M _d	0.051	0.413	0.95	0.294	0.04
M _D	0.048	0.404	0.92	0.283	1.16
M _{dm}	0.048	0.432	0.89	0.270	0.08
M _{DM}	0.047	0.403	0.89	0.266	13.42

Table 1: Admin1 level (areal) validation results.

Perhaps this is due in part to the large amount of positional uncertainty in the MICS data, making predictions for left out MICS data harder than for DHS data.

It is also possible that the lack of improvement in model performance when including MICS data is due in part to the increased reliance on the urbanicity classification based on population density. While we use population density estimates from WorldPop to classify pixels as urban/rural at 5km resolution, our designations almost certainly do not match up perfectly with official ones, which are unknown except for at the sampled clusters. We assume urban MICS clusters can only be in the part of the geomasked area we classify as urban. The same is true for rural MICS clusters. This is not the case, however, for the

DHS clusters, since we know the DHS cluster locations with a high degree of accuracy, and, for example, an urban DHS cluster might not be near any pixels we classify as urban.

Note that, while the M_{DM} approach took significantly longer than the others in Table 1 with an average runtime of 13.42 minutes, this runtime is much better than the runtime of [Wilson and Wakefield \(2021\)](#). The method proposed in [Wilson and Wakefield \(2021\)](#) took approximately 52 hours to run 1000 MCMC iterations with only 398 surveyed clusters. This indicates that our proposed method for accounting for positional uncertainty can help to improve computation time substantially compared to MCMC based methods.

5. Application to women’s secondary education

We apply the M_d , M_D , and M_{DM} approaches to women’s secondary education in Nigeria using both the 2018 NDHS and the 2016 NMICS. Posterior means along with 95% CI widths are plotted spatially at the 5km pixel, Admin2, and Admin1 levels in Figures 4-6. Parameter posterior summary statistics for these approaches are given in Table 2.

Differences in parameter estimates are most pronounced between the M_{DM} approach and the others. The M_d and M_D approaches have fairly similar parameter estimates with moderate differences in the estimates (and 95% CI widths) of the urban effect, 0.33 (0.49) and 0.49 (0.44) respectively, and cluster variance, 1.41 (0.39) and 1.33 (0.39) respectively, and a slight difference in the estimate of the effect of healthcare inaccessibility, -0.20 (0.21) and -0.14 (0.18) respectively. The M_{DM} approach, however, estimated the urban effect to be much higher with a posterior mean (and 95% CI width) of 1.03 (0.32), and estimated the effect of population density to be much weaker, i.e. 0.44 (0.28), as compared to the M_d and M_D approaches with estimated population density effects of 0.82 (0.42) and 0.80 (0.38) respectively. These larger differences reflect the inclusion of the MICS survey in the M_{DM} approach, and perhaps also some slight differences in the target populations of the DHS and MICS surveys. It is also possible that

these differences in parameter estimates reflect the increased reliance that comes with larger positional uncertainty on the assumed prior for the spatial positions of the clusters, as mentioned in the previous section.

Similarly, the M_d and M_D approaches largely agree in terms of their predictions and CI widths, whereas the M_{DM} approach has similar, albeit noticeably different, predictions. In addition, the CI widths for predictions at all aggregations levels are much smaller for the M_{DM} approach than for the other approaches. We found this to be generally true at all aggregation levels. While it may be tempting to attribute the smaller CI widths of the M_{DM} approach to it utilizing more information, and to conclude that the M_{DM} approach predictions are better, the validation from Section 4 suggests a more nuanced interpretation. We found the reduced CI widths of the M_{DM} approach to be more anti-conservative than the CI widths of the other approaches rather than necessarily leading to more accurate estimates.

	M_{DM}		M_D		M_d	
	Est	95% CI	Est	95% CI	Est	95% CI
(Int)	-1.24	(-1.40, -0.99)	-1.66	(-1.90, -1.33)	-1.69	(-1.93, -1.37)
Urban	1.03	(0.86, 1.18)	0.49	(0.26, 0.70)	0.33	(0.09, 0.58)
Healthcare Inaccessibility	-0.05	(-0.11, 0.01)	-0.14	(-0.23, -0.05)	-0.20	(-0.30, -0.09)
Elevation	0.05	(-0.02, 0.14)	0.15	(0.02, 0.27)	0.15	(0.02, 0.28)
Dist. Rivers & Lakes	0.02	(-0.06, 0.10)	0.09	(-0.03, 0.21)	0.10	(-0.02, 0.22)
Population	0.44	(0.30, 0.58)	0.80	(0.60, 0.98)	0.82	(0.60, 1.02)
σ^2	0.54	(0.33, 0.84)	0.60	(0.36, 0.98)	0.62	(0.38, 0.98)
ϕ	0.87	(0.51, 0.99)	0.84	(0.47, 0.99)	0.85	(0.47, 0.99)
σ_ϵ^2	1.47	(1.29, 1.66)	1.33	(1.14, 1.53)	1.41	(1.24, 1.63)

Table 2: Posterior parameter central estimates and 95% credible intervals for three approaches considered. Covariates are transformed and normalized as described in Section 2.2.

6. Conclusions

In this paper, we propose a new geostatistical model capable of accounting for multiple kinds of anonymization of spatial positions, including both jitter-

ing and geomasking. It can also be performed relatively quickly compared to alternative methods suitable for such contexts such as those involving MCMC. It is more flexible in terms of the kinds of positional anonymization allowed, the likelihood families allowed, and the method by which integration points and weights are automatically constructed based directly on the distributional form of the positional uncertainty resulting from the anonymization. While the focus of this paper is to apply the proposed model to DHS and MICS data, its flexibility makes it applicable in other settings as well, such as when modeling MICS data without DHS data, or in other contexts with positional uncertainty.

We demonstrate via validation that using this method to account for positional anonymization can improve predictions, and at least did not make them worse compared to when positional anonymization was not accounted for. We recommend the proposed method particularly in cases where the modeler wishes to model DHS and MICS surveys jointly, and in situations where the spatial random effects do not vary substantially over spatial scales on which the uncertain observation positions may vary, such as within geomasked areas. In addition, it may be useful in contexts where spatial covariates vary significantly as a function of the uncertain observation positions. In these settings, we find that accounting for positional uncertainty using the proposed model generally improves areal predictions.

Due to the importance of fine scale spatial modeling of health and demographic indicators, methods for improving identifiability in cases where spatial random effects may vary significantly on fine spatial scales warrant further study. In addition, it is possible that accounting for uncertainty from urbanicity classification may improve predictions, although that is a complex problem beyond the scope of this work. More generally, we believe an interesting avenue of future work in this context would be to study the inferential effects of uncertain spatial covariates correlated with the modeled response, since these covariates may inform both the response and the spatial positions of the observations.

In addition, our results suggest that DHS surveys' jittered cluster positions may lead to more stable and generally improved inference when compared to

MICS surveys' geomasked cluster positions due to the relatively small level of positional uncertainty resulting from jittering in DHS data. This is particularly the case when estimating health and demographic indicators at fine spatial scales, an increasingly emphasized aspect of the UN sustainable development goals. We therefore advocate for survey positional anonymization methods to be chosen in tandem with goals for the spatial resolution of prediction where possible.

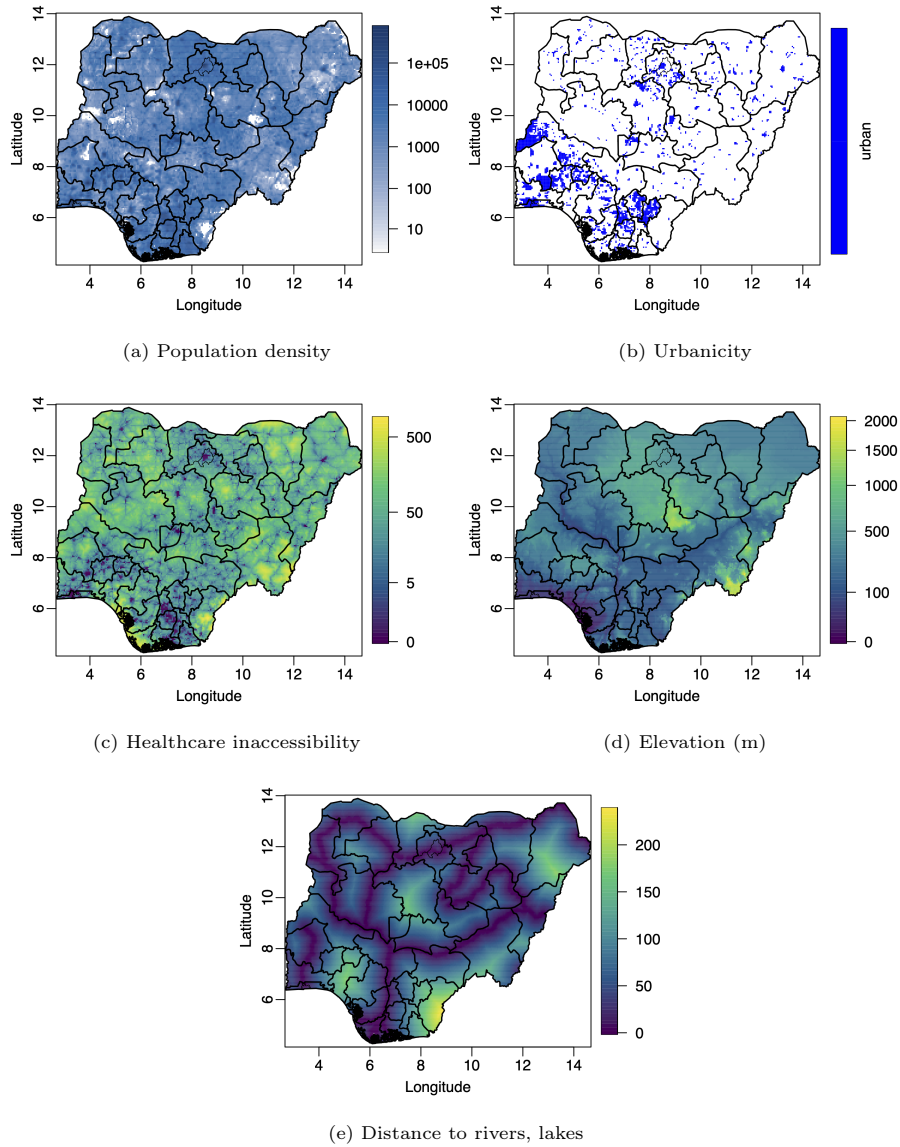


Figure 3: Covariates included in the analysis prior to transformation. Admin1 areas and 6 senatorial districts are outlined in thick and thin lines respectively. Color scales are transformed using the transformations associated with each covariate.

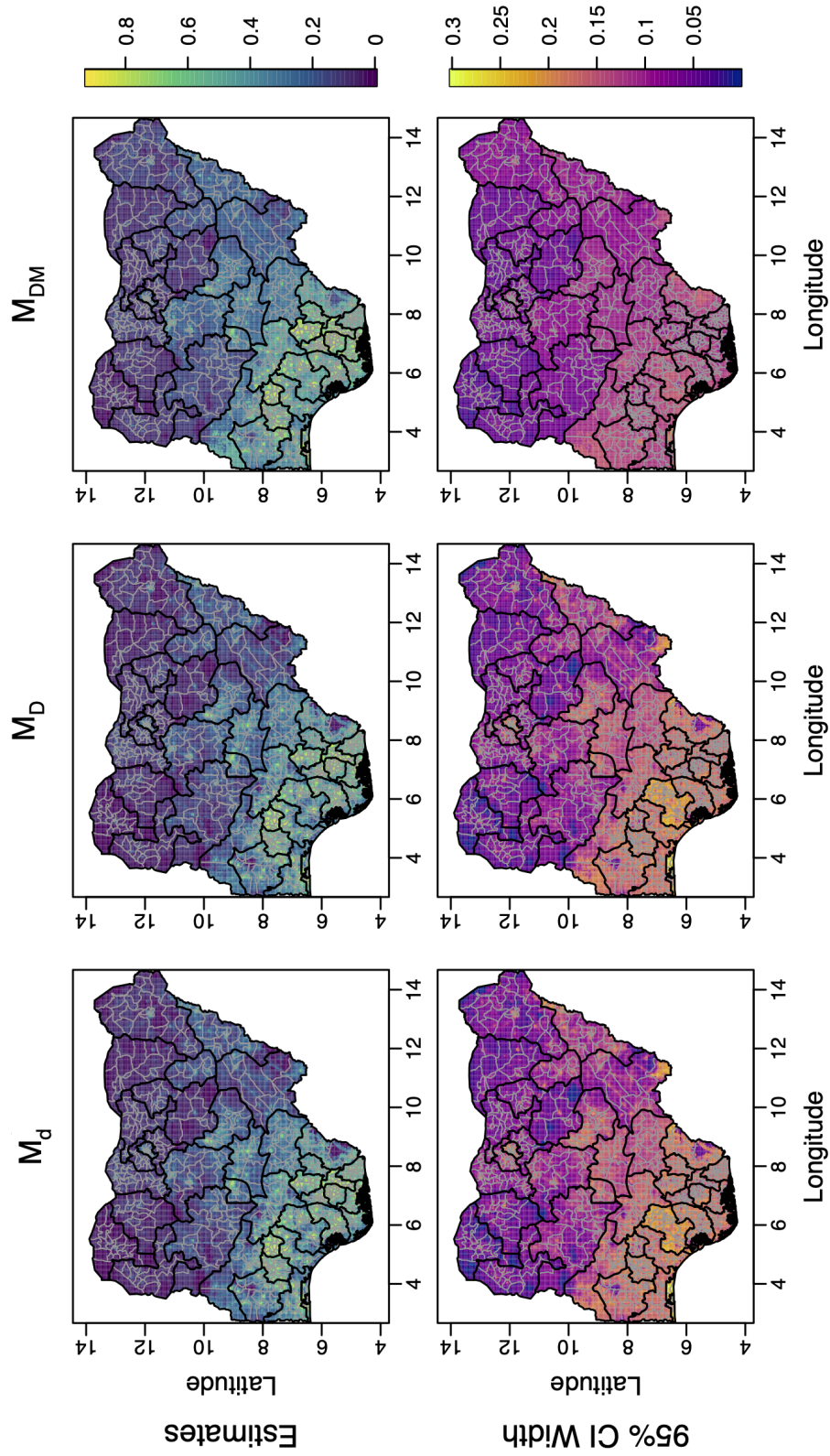


Figure 4: 5km pixel level women's secondary education prevalence predictions (top row) and 95% credible interval widths (bottom row). Admin2 area boundaries are given in light grey while MICS stratum boundaries are given in black.

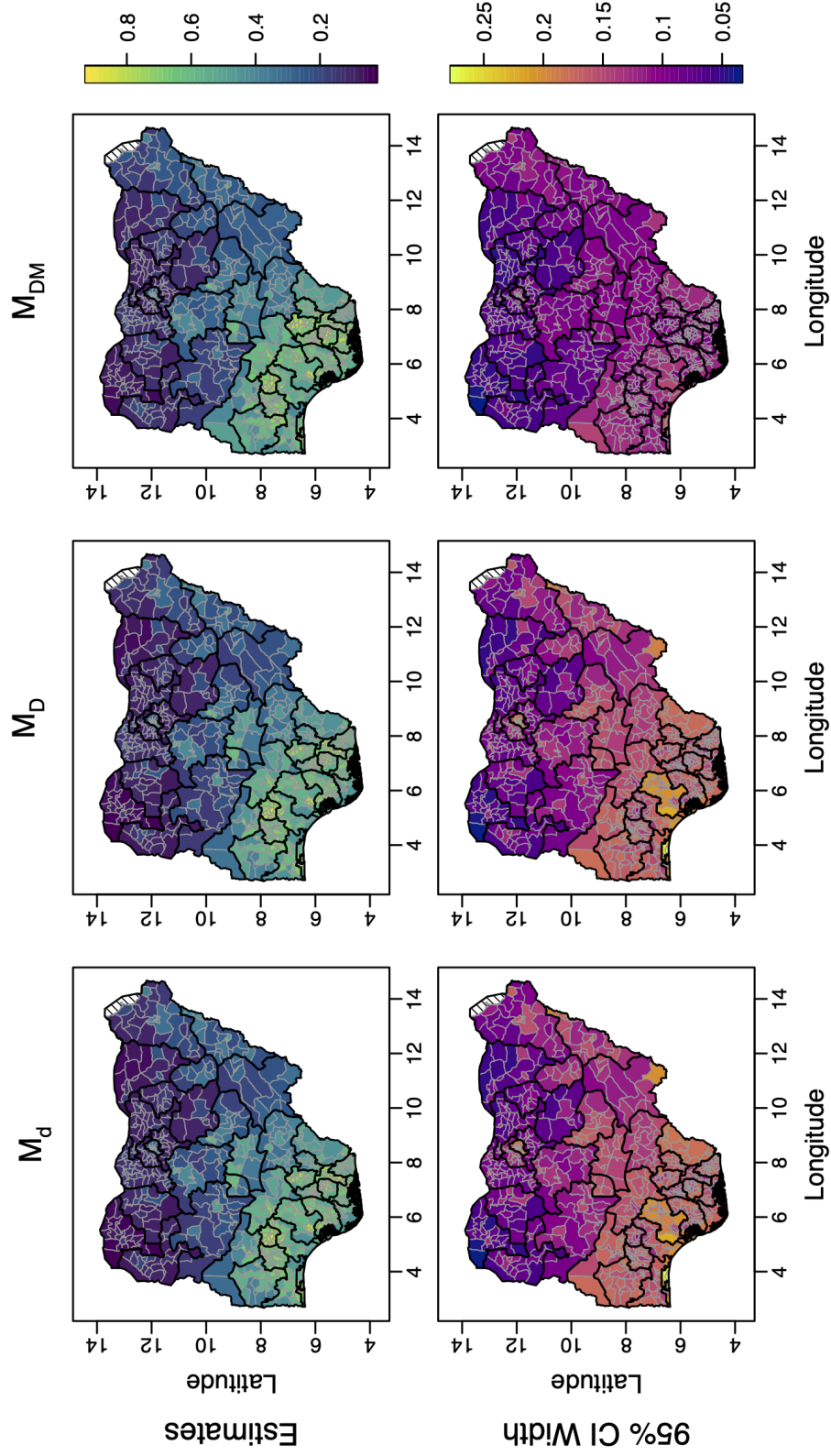


Figure 5: Admin2 level women's secondary education prevalence predictions (top row) and 95% credible interval widths (bottom row). Admin2 area boundaries are given in light grey while MICS stratum boundaries are given in black.

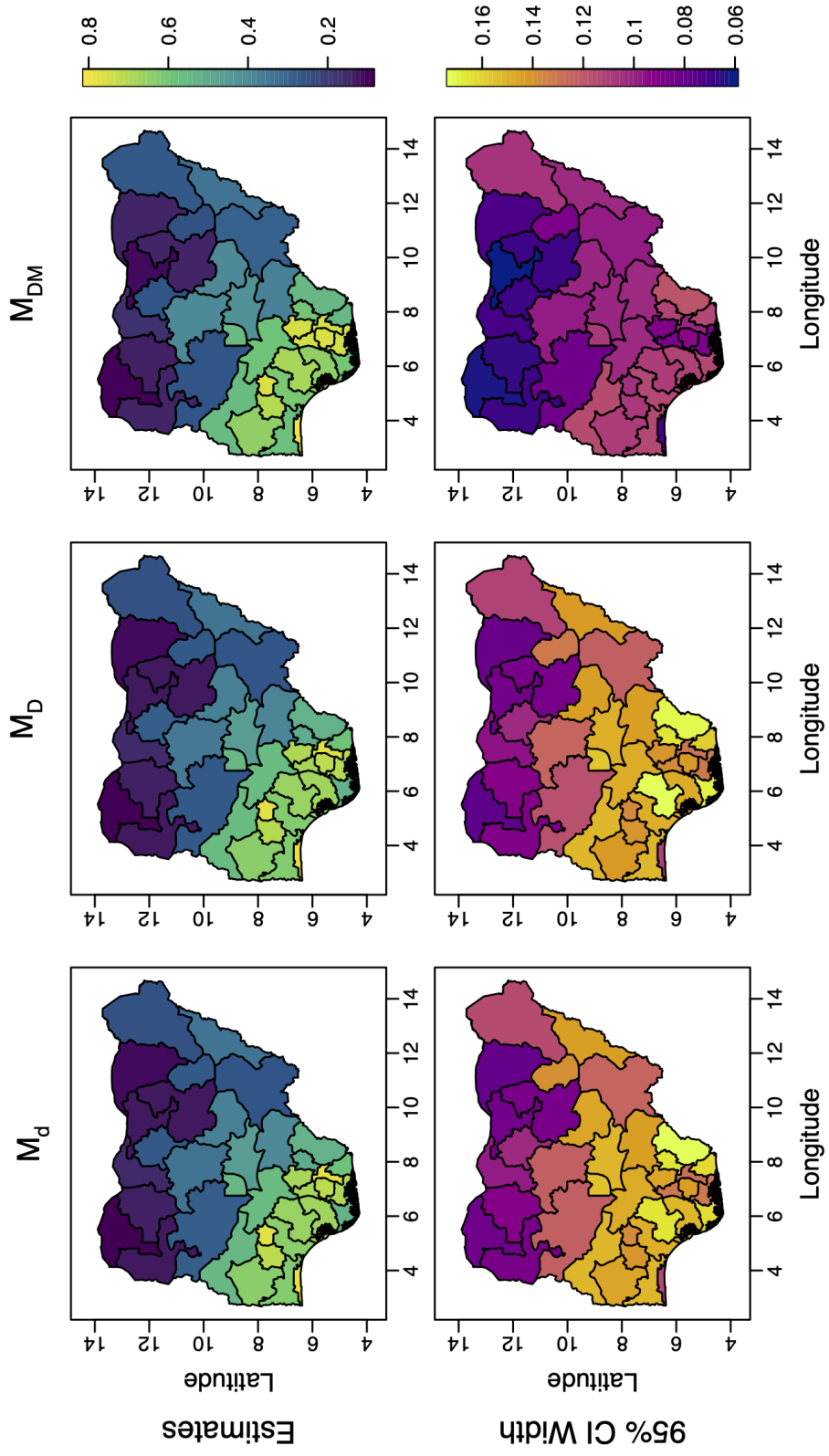


Figure 6: Admin1 level women's secondary education prevalence predictions (top row) and 95% credible interval widths (bottom row).

References

- Altay, U., Paige, J., Riebler, A., Fuglstad, G.A., 2022. Fast geostatistical inference under positional uncertainty: Analysing DHS household survey data. arXiv preprint arXiv:2202.11035 .
- Altay, U., Paige, J., Riebler, A., Fuglstad, G.A., 2024. Impact of jittering on raster-and distance-based geostatistical analyses of DHS data. *Statistical Modelling* , 1471082X231219847.
- Binder, D., 1983. On the variances of asymptotically normal estimators from complex surveys. *International Statistical Review* 51, 279–292.
- Bolgrien, A., Boyle, E.H., Sobek, M., King, M., 2024. IPUMS MICS Data Harmization Code. Version 1.1 [Stata Syntax]. Technical Report. IPUMS. Minneapolis, MN. doi:<https://doi.org/10.18128/D082.V1.1>.
- Burgert, C.R., Colston, J., Roy, T., Zachary, B., 2013. Geographic displacement procedure and georeferenced data release policy for the Demographic and Health Surveys. <https://dhsprogram.com/pubs/pdf/SAR7/SAR7.pdf>. DHS Spatial Analysis Reports No. 7.
- Burstein, R., Wang, H., Reiner Jr, R.C., Hay, S.I., 2018. Development and validation of a new method for indirect estimation of neonatal, infant, and child mortality trends using summary birth histories. *PLoS Medicine* 15, e1002687.
- Carroll, R.J., Ruppert, D., Crainiceanu, C.M., Stefanski, L.A., 2006. *Measurement Error in Nonlinear Models: A Modern Perspective*. Chapman and Hall/CRC.
- Cressie, N., Kornak, J., 2003. Spatial statistics in the presence of location error with an application to remote sensing of the environment. *Statistical Science* , 436–456.

- Devarajan, S., 2013. Africa's statistical tragedy. *Review of Income and Wealth* 59, S9–S15.
- Fanshawe, T., Diggle, P., 2011. Spatial prediction in the presence of positional error. *Environmetrics* 22, 109–122.
- Fronterrière, C., Giorgi, E., Diggle, P.J., 2018. Geostatistical inference in the presence of geomasking: a composite-likelihood approach. *Spatial Statistics* Available online, June 23, 2018.
- Gascoigne, C., Smith, T., Paige, J., Wakefield, J., 2023. Estimating subnational under-five mortality rates using a spatio-temporal age-period-cohort model. arXiv preprint arXiv:2309.02093 .
- Geyer, C.J., Meeden, G.D., 2005. Fuzzy and randomized confidence intervals and p-values. *Statistical Science* 20, 358–366.
- Gneiting, T., Raftery, A.E., 2007. Strictly proper scoring rules, prediction, and estimation. *Journal of the American Statistical Association* 102, 359–378.
- Godwin, J., Wakefield, J., 2021. Space-time modeling of child mortality at the Admin-2 level in a low and middle income countries context. *Statistics in Medicine* 40, 1593–1638.
- Gómez-Rubio, V., Rue, H., 2018. Markov chain Monte Carlo with the integrated nested Laplace approximation. *Statistics and Computing* 28, 1033–1051.
- Graetz, N., Friedman, J., Osgood-Zimmerman, A., Burstein, R., Biehl, M.H., Shields, C., Mosser, J.F., Casey, D.C., Deshpande, A., Earl, L., Reiner, R., Ray, S., Fullman, N., Levine, A., Stubbs, R., Mayala, B., Longbottom, J., Browne, A., Bhatt, S., Weiss, D., Gething, P., Mokdad, A., Lim, S., Murray, C., Gakidou, E., Hay, S., 2018. Mapping local variation in educational attainment across Africa. *Nature* 555, 48–53.
- Horvitz, D., Thompson, D., 1952. A generalization of sampling without replacement from a finite universe. *Journal of the American Statistical Association* 47, 663–685.

- ICF International, 2012. Demographic and Health Survey Sampling and Household Listing Manual. Calverton, Maryland, USA: ICF International.
- Jerven, M., 2013. Poor numbers: how we are misled by African development statistics and what to do about it. Cornell University Press.
- Khan, S., Hancioglu, A., 2019. Multiple indicator cluster surveys: delivering robust data on children and women across the globe. *Studies in Family Planning* 50, 279–286.
- LBD Child Growth Failure Collaborators and others, 2020. Mapping local patterns of childhood overweight and wasting in low-and middle-income countries between 2000 and 2017. *Nature medicine* 26, 750–759.
- Li, Z.R., Hsiao, Y., Godwin, J., Martin, B.D., Wakefield, J., Clark, S.J., 2019. Changes in the spatial distribution of the under five mortality rate: small-area analysis of 122 DHS surveys in 262 subregions of 35 countries in Africa. *PLoS one* 14. Published January 22, 2019.
- Lumley, T., 2023. survey: analysis of complex survey samples. R package version 4.2-1.
- Lumley, T., Scott, A., 2017. Fitting regression models to survey data. *Statistical Science* .
- Marquez, N., Wakefield, J., 2021. Harmonizing child mortality data at disparate geographic levels. *Statistical Methods in Medical Research* 30, 1187–1210.
- National Bureau of Statistics (NBS) and United Nations Children’s Fund (UNICEF), 2017. Multiple Indicator Cluster Survey 2016-17, Survey Findings Report. Technical Report. National Bureau of Statistics and United Nations Children’s Fund. Abuja, Nigeria.
- National Oceanic and Atmospheric Administration, 2022. National centers for environmental information. URL: <https://www.ngdc.noaa.gov/mgg/topo/gltiles.html>.

National Population Commission (NPC) [Nigeria] and ICF, 2019. Nigeria Demographic and Health Survey 2018. Technical Report. NPC and ICF. Abuja, Nigeria and Rockville, Maryland, USA.

Natural Earth, 2012. Rivers + lake centerlines. URL: <http://www.naturalearthdata.com/downloads/10m-physical-vectors/10m-rivers-lake-centerlines>.

Osgood-Zimmerman, A., Millear, A.I., Stubbs, R.W., Shields, C., Pickering, B.V., Earl, L., Graetz, N., Kinyoki, D.K., Ray, S.E., Bhatt, S., Browne, A., Burstein, R., Cameron, E., Casey, D., Deshpande, A., Fullman, N., Gething, P., Gibson, H., Henry, N., Herrero, M., Krause, L., Letourneau, I., Levine, A., Liu, P., Longbottom, J., Mayala, B., Mosser, J., Noor, A., Pigott, D., Piwoz, E., Rao, P., Rawat, R., Reiner, R., Smith, D., Weiss, D., Wiens, K., Mokdad, A., S.S., L., Murray, C., Kassebaum, N., Hay, S., 2018. Mapping child growth failure in Africa between 2000 and 2015. *Nature* 555, 41–47.

Paige, J., Fuglstad, G.A., Riebler, A., Wakefield, J., 2022a. Bayesian multiresolution modeling of georeferenced data: An extension of ‘LatticeKrig’. *Computational Statistics & Data Analysis* 173, 107503.

Paige, J., Fuglstad, G.A., Riebler, A., Wakefield, J., 2022b. Design- and model-based approaches to small-area estimation in a low and middle income country context: Comparisons and recommendations. *Journal of Survey Statistics and Methodology* 10, 50–80.

Paige, J., Fuglstad, G.A., Riebler, A., Wakefield, J., 2022c. Spatial aggregation with respect to a population distribution: Impact on inference. *Spatial Statistics* 52, 100714.

Perez-Heydrich, C., Warren, J.L., Burgert, C.R., Emch, M., 2013. Guidelines on the use of DHS GPS data. ICF International.

Riebler, A., Sørbye, S., Simpson, D., Rue, H., 2016. An intuitive Bayesian spatial

- model for disease mapping that accounts for scaling. *Statistical Methods in Medical Research* 25, 1145–1165.
- Sandefur, J., Glassman, A., 2015. The political economy of bad data: Evidence from African survey and administrative statistics. *The Journal of Development Studies* 51, 116–132.
- Simpson, D., Rue, H., Riebler, A., Martins, T., Sørbye, S., 2017. Penalising model component complexity: A principled, practical approach to constructing priors (with discussion). *Statistical Science* 32, 1–28.
- United Nations, 2020. Sustainable Development Goals. <http://sustainabledevelopment.un.org/owg.html>.
- USAID, 2024. The DHS Program - Quality information to plan, monitor, and improve population, health, and nutrition programs. United States Agency for International Development. <http://www.dhsprogram.com>.
- Wagner, Z., Heft-Neal, S., Bhutta, Z.A., Black, R.E., Burke, M., Bendavid, E., 2018. Armed conflict and child mortality in Africa: a geospatial analysis. *The Lancet* .
- Weiss, D.J., Nelson, A., Gibson, H., Temperley, W., Peedell, S., Lieber, A., Hancher, M., Poyart, E., Belchior, S., Fullman, N., et al., 2018. A global map of travel time to cities to assess inequalities in accessibility in 2015. *Nature* 553, 333–336.
- Wilson, K., Wakefield, J., 2021. Estimation of health and demographic indicators with incomplete geographic information. *Spatial and Spatio-temporal Epidemiology* 37, 100421.
- World Pop, 2022. Open spatial demographic data and research. URL: <https://hub.worldpop.org>.
- Wu, Y., Li, Z.R., Mayala, B.K., Wang, H., Gao, P., Paige, J., Fuglstad, G.A., Moe, C., Godwin, J., Donohue, R.E., Croft, T.N.,

Wakefield, J., 2021. Spatial Modeling for Subnational Administrative Level 2 Small-Area Estimation. Technical Report. DHS Spatial Analysis Reports No. 21. URL: <https://dhsprogram.com/publications/publication-SAR21-Spatial-Analysis-Reports.cfm>.

Supplementary materials for 'Spatial fusion under positional error and geomasking'

John Paige^{a,*}, Geir-Arne Fuglstad^a, Andrea Riebler^a

^a*Department of Mathematical Sciences, NTNU, Trondheim, Norway*

S.1. MICS positional error integration scheme

In order to evaluate (3), we use a different numerical scheme for MICS data than for DHS data due to the differing positional uncertainty distributions. We will make the assumption that $\pi(s_c, t_c = t)$ and $\pi(y_c | r(t))$ are both continuous in t almost everywhere for each c . Note that, in the case of geomasking, $\pi(s_c, t_c = t) = \pi(s_c | t_c = t) \cdot \pi(t_c = t)$ where $\pi(s_c | t_c = t) = \mathbb{I}\{s_c \ni t\}$, and we assume $\pi(t)$ is proportional to population density, so the assumptions on continuity hold.

Our integration scheme can be derived by rewriting the integral in (3) in terms of a sum of integrals over 'integration zones' that partition the support of $\pi(s_c, t_c)$, say, $Z \subset \mathbb{R}^2$, for any fixed cluster c (although Z can be in more general spaces than \mathbb{R}^2). In our case we can think of Z as the geomasked area containing s_c , or, more generally, as the set of possible points where the true location of cluster c might be located. Rewriting the integral in (3), we get:

$$\begin{aligned}\pi(y_c | r(\cdot)) &= \int_Z \pi(y_c | r(t_c)) \pi(s_c | t_c) \pi(t_c) dt_c \\ &= \sum_{k=1}^K \int_{Z^k} \pi(y_c | r(t_c)) \pi(s_c | t_c) \pi(t_c) dt_c,\end{aligned}\tag{A.1}$$

where $Z^1 \cup \dots \cup Z^K = Z$ are the aforementioned integration zones forming a partition of Z . Note that any single Z^k need not be spatially contiguous. Our goal will be to select a single integration point in each zone Z^k that is 'representative' in some sense of Z^k , and to choose each integration zone Z^k carefully so that $\pi(y_c | r(t_c))$ remains relatively constant throughout each zone as a function of t_c .

To set the integration zones and their representative points, we first construct a fine spatial grid, $G = \{g_1, \dots, g_{|G|}\}$ within Z . We then consider the transformation of the spatial grid points to an alternative space where distances better represent variations in the integrand. For now, we assume the grid points are transformed via $\mathbf{h}(\cdot) = \mathbf{d}(\cdot)$, which is a transformation from spatial location to the vector of covariates at the location. The transformed grid points are given by $X = \{\mathbf{x}_1, \dots, \mathbf{x}_{|G|}\} = \{\mathbf{h}(g_1), \dots, \mathbf{h}(g_{|G|})\}$,

*Corresponding author

Email address: john.paige@ntnu.no (John Paige)

where $|G|$ denotes the cardinality of G , i.e. the number of fine grid points. We discuss other choices of $\mathbf{h}(\cdot)$ accounting for correlation due to spatial random effects later in this section.

We then wish to choose our set of K representative points from among the $|G|$ grid points, along with their associated K integration zones, by minimizing the criterion,

$$\mathbf{x}_1^*, \dots, \mathbf{x}_K^*, X^1, \dots, X^K = \underset{\mathbf{x}_1^*, \dots, \mathbf{x}_K^*, X^1, \dots, X^K}{\operatorname{argmin}} \sum_{k=1}^K \sum_{\mathbf{h}(g) \in X^k} \pi(s_c | t_c = g) \pi(t_c = g) \|\mathbf{x}_k^* - \mathbf{h}(g)\|^2, \quad (\text{A.2})$$

under the constraints that $X^1 \cup \dots \cup X^K = X$ form a partition of the transformed fine grid, X , and that $\mathbf{x}_k^* \in X^k$ for $k = 1, \dots, K$.

Now we can back-transform to the spatial domain, taking $\tilde{t}_{c1} \equiv \mathbf{h}^{-1}(\mathbf{x}_1^*), \dots, \tilde{t}_{cK} \equiv \mathbf{h}^{-1}(\mathbf{x}_K^*)$, and defining a partition of the fine spatial grid $G^1 \cup \dots \cup G^K = G$, where each G^k is the preimage of X^k under $\mathbf{h}(\cdot)$, so that $G^k \equiv \{g : \mathbf{h}(g) \in X^k\}$ for $k = 1, \dots, K$. By the definition of the optimization criterion in (A.2), each \tilde{t}_{ck} is chosen to have similar covariate values to the other fine grid points in G^k , which means that the covariate values of each of the points in G^k tend to be similar, with \tilde{t}_{ck} being the most representative point in G^k .

Note that if \mathbf{h} is not invertible so that $\mathbf{h}^{-1}(\mathbf{x}_k^*) = \{g_{i_1}, \dots, g_{i_k}\}$ for some k , then we can set \tilde{t}_{ck} to be any element of $\mathbf{h}^{-1}(\mathbf{x}_k^*)$ arbitrarily.

In the case of geomasked data, (A.2) then simplifies to:

$$\mathbf{x}_1^*, \dots, \mathbf{x}_K^*, X^1, \dots, X^K = \underset{\mathbf{x}_1^*, \dots, \mathbf{x}_K^*, X^1, \dots, X^K}{\operatorname{argmin}} \sum_{k=1}^K \sum_{\mathbf{h}(g) \in X^k} q(g) \|\mathbf{x}_k^* - \mathbf{h}(g)\|^2. \quad (\text{A.3})$$

Here, $q(g)$ is the population density associated with spatial location g , and the criterion is the same for all clusters in the same geomasked area. Hence, while (A.2) must be minimized for each cluster, (A.3) only needs to be minimized for each geomasked area, leading to substantial computational savings. The K -medoids algorithm and the related partitioning around medoids (PAM) algorithm [1] were built to solve minimization problems taking the form of (A.2) and (A.3).

We then define the integration weights α_{ck} , $k = 1, \dots, K$ to be proportional to the average joint density of s_c and t_c associated with the k -th representative point (medoid) divided by the joint positional density evaluated at the medoid, i.e.,

$$\alpha_{ck} = \frac{1}{\pi(s_c | t_c = \tilde{t}_{ck}) \pi(t_c = \tilde{t}_{ck})} \sum_{g \in G^k} \pi(s_c | t_c = g) \pi(t_c = g). \quad (\text{A.4})$$

In the case of the geomasked MICS data, this simplifies to the average population density associated with medoid k divided by the population density evaluated at the medoid:

$$\alpha_{ck} = \frac{1}{q(\tilde{t}_{ck})} \sum_{g \in G^k} q(g). \quad (\text{A.5})$$

Just as for the integration points, in the case of geomasking the integration weights need only be calculated once for each of the geomasked areas rather than once for each cluster.

If $\pi(y_c | r(t_c))$ were constant as a function of t_c in each zone Z^k , then for any $k = 1, \dots, K$, we can plug in the expression for α_{ck} from (A.4) back into (A.1) to get:

$$\begin{aligned} \int_{Z^k} \pi(y_c | r(t_c)) \pi(s_c | t_c) \pi(t_c) dt_c &= \pi(y_c | r(\tilde{t}_{ck})) \int_{Z^k} \pi(s_c | t_c) \pi(t_c) dt_c \\ &\approx \pi(y_c | r(\tilde{t}_{ck})) \sum_{g \in G^k} \pi(s_c | t_c = g) \pi(t_c = g) \\ &= \alpha_{ck} \pi(y_c | r(\tilde{t}_{ck})) \pi(s_c | \tilde{t}_{ck}) \pi(\tilde{t}_{ck}), \end{aligned}$$

and so

$$\sum_{k=1}^K \int_{Z^k} \pi(y_c | r(t_c)) \pi(s_c | t_c) \pi(t_c) dt_c \approx \sum_{k=1}^K \alpha_{ck} \pi(y_c | r(\tilde{t}_{ck})) \pi(s_c | \tilde{t}_{ck}) \pi(\tilde{t}_{ck}),$$

yielding the integration scheme in (4). Our approximation is therefore accurate when $\pi(y_c | r(t_c))$ varies little for $t_c \in Z^k$, and when $\int_{Z^k} \pi(s_c | t_c) \pi(t_c) dt \approx \sum_{g \in G^k} \pi(s_c | t_c = g) \pi(t_c = g)$. The former will be the case for small enough Z^k provided $\pi(y_c | r(t_c))$ is continuous in t_c almost everywhere in Z^k . Importantly, $\pi(y_c | r(t_c))$ could be discontinuous at the boundaries of Z^k , as can be the case for the MICS data since Z is chosen to be the urban or rural part of an area, and urbanicity, which influences $\pi(y_c | r(t_c))$, is discontinuous. Even if Z itself is not chosen in a way to account for such discontinuities in $r(t_c)$, for large enough K , the clustering algorithm will choose the Z^k automatically so that the discontinuities do not occur within them.

Note that spatial information can be incorporated into this integration scheme as well. For a continuous spatial model, for example, the same integration scheme can be applied using transformation $\mathbf{d}^*(s; \lambda) = (\lambda s^T \mathbf{d}(s)^T)^T$ in lieu of $\mathbf{d}(s)$, since this encourages integration points to be more spread out spatially within Z , and λ can be chosen, for example, as the prior effective range divided by the diameter of the spatial domain, \mathcal{D} , or to match the range of the covariates. The parameter λ can also be increased until the chosen sets $G^1, \dots, G^{K^{\text{MICS}}}$ are fully connected if necessary. For an areal spatial model with spatial random effects occurring at finer scales than the positional uncertainty distribution (i.e. finer than the geomasked area), one could set $\mathbf{d}^*(s; \lambda) = (\lambda \mathbf{a}(A^*[s])^T \mathbf{d}(s)^T)^T$, where $A^*[s]$ is the index of the specific areal spatial effect containing s , and $\mathbf{a}(\cdot)$ could be a function returning the spatial coordinates of the centroid of the area. The parameter λ could be chosen in ways similar to the continuous spatial case, or in order to ensure that there are sufficient integration points in each modeled area.

S.1.1. Constructing the integration scheme: Illustration for FCT Abuja

To illustrate selecting the MICS integration points for FCT Abuja, we first choose $K = 25$, and select a fine grid with 1km resolution. The resulting fine grid and integration points are depicted along with covariates in Figure A.3. In the Figure, the integration points are chosen to be representative of the different combinations of covariate values throughout the area. As K increases, the grouping of fine grid integration points becomes more refined as illustrated in Figure A.4 for $K = 3, 6, 12$, and 24. Computation and memory requirements increase linearly with the number of integration points per sampled cluster,

but the accuracy of the integration improves as well. We also compare the integration scheme for $K = 25$ with raster based covariates used in the analysis in Figure A.3.

S.2. PC prior for proportion of structured variance

The PC prior for the BYM2 parameter representing the proportion of structured variance takes the form:

$$f(\phi) = \lambda \exp(-\lambda d(\phi)) \left| \frac{\partial d(\phi)}{\partial \phi} \right|$$

$$d(\phi) = \sqrt{2\text{KLD}(\phi)},$$

where $d(\cdot)$ is the Kullback Liebler Divergence (KLD) distance, and the KLD is:

$$\begin{aligned} \text{KLD}(\phi) &= \frac{1}{2} \left[\text{tr} \left((1 - \phi)I + \phi \mathbf{Q}_\star^{-1} \right) - n - \log \left| (1 - \phi)I + \phi \mathbf{Q}_\star^{-1} \right| \right] \\ &= \frac{1}{2} \left[n(1 - \phi) + \phi \text{tr}(\mathbf{Q}_\star^{-1}) - n - \log \left| (1 - \phi)I + \phi \mathbf{Q}_\star^{-1} \right| \right] \\ &= \frac{n\phi}{2} \left(\frac{1}{n} \text{tr}(\mathbf{Q}_\star^{-1}) - 1 \right) - \frac{1}{2} \log \left| (1 - \phi)I + \phi \mathbf{Q}_\star^{-1} \right| \\ &= \frac{n\phi}{2} \left(\left(\frac{1}{n} \sum_{i=1}^n \tilde{\gamma}_i \right) - 1 \right) - \frac{1}{2} \log \prod_{i=1}^n (1 + (\tilde{\gamma}_i - 1)\phi) \\ &= \frac{n\phi}{2} \left(\left(\frac{1}{n} \sum_{i=1}^n \tilde{\gamma}_i \right) - 1 \right) - \frac{1}{2} \sum_{i=1}^n \log(1 + (\tilde{\gamma}_i - 1)\phi). \end{aligned}$$

Here, $\tilde{\gamma}_i$ is an eigenvalue for \mathbf{Q}_\star^{-1} :

$$\tilde{\gamma}_i = 1/\gamma_i \quad \text{for } \gamma_i \text{ eigenvalues of } \mathbf{Q}_\star.$$

The PC prior Jacobian factor depends on the derivative of the KLD with respect to ϕ , which is:

$$\begin{aligned} \left| \frac{\partial \text{KLD}(\phi)}{\partial \phi} \right| &= \left| \frac{\partial}{\partial \phi} \left[\frac{n\phi}{2} \left(\left(\frac{1}{n} \sum_{i=1}^n \tilde{\gamma}_i \right) - 1 \right) - \frac{1}{2} \sum_{i=1}^n \log(1 + (\tilde{\gamma}_i - 1)\phi) \right] \right| \\ &= \left| \frac{n}{2} \left(\left(\frac{1}{n} \sum_{i=1}^n \tilde{\gamma}_i \right) - 1 \right) - \frac{1}{2} \sum_{i=1}^n \frac{\partial}{\partial \phi} \log(1 + (\tilde{\gamma}_i - 1)\phi) \right| \\ &= \left| \frac{1}{2} \sum_{i=1}^n \tilde{\gamma}_i - \frac{n}{2} - \frac{1}{2} \sum_{i=1}^n \frac{\tilde{\gamma}_i - 1}{1 + (\tilde{\gamma}_i - 1)\phi} \right|. \end{aligned}$$

We therefore find the Jacobian factor is:

$$\begin{aligned} \left| \frac{\partial d(\phi)}{\partial \phi} \right| &= \frac{1}{2} \frac{1}{\sqrt{2\text{KLD}(\phi)}} \left| \frac{\partial 2\text{KLD}(\phi)}{\partial \phi} \right| \\ &= \frac{1}{2\sqrt{2\text{KLD}(\phi)}} \left| \sum_{i=1}^n \tilde{\gamma}_i - n - \sum_{i=1}^n \frac{\tilde{\gamma}_i - 1}{1 + (\tilde{\gamma}_i - 1)\phi} \right|. \end{aligned}$$

The PC prior for ϕ is therefore,

$$f(\phi) = \lambda \exp(-\lambda d(\phi)) \frac{1}{2\sqrt{2\text{KLD}(\phi)}} \left| \sum_{i=1}^n \tilde{\gamma}_i - n - \sum_{i=1}^n \frac{\tilde{\gamma}_i - 1}{1 + (\tilde{\gamma}_i - 1)\phi} \right|, \quad (\text{B.1})$$

with cdf,

$$F(\phi) = 1 - \exp(-\lambda d(\phi)). \quad (\text{B.2})$$

S.3. Additional validation results

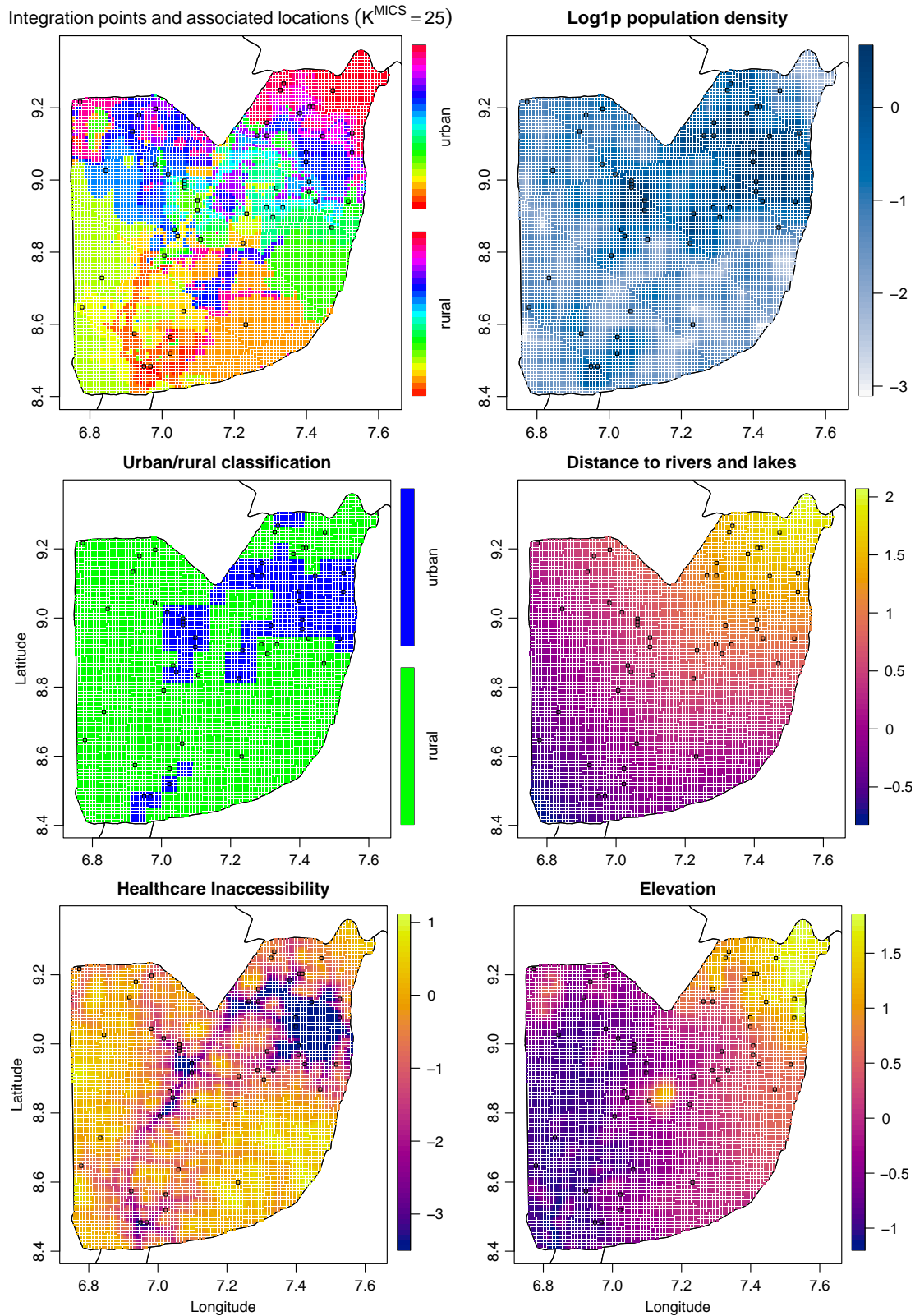
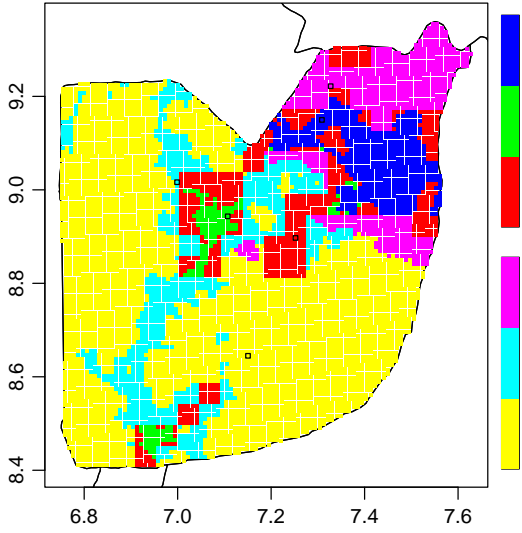
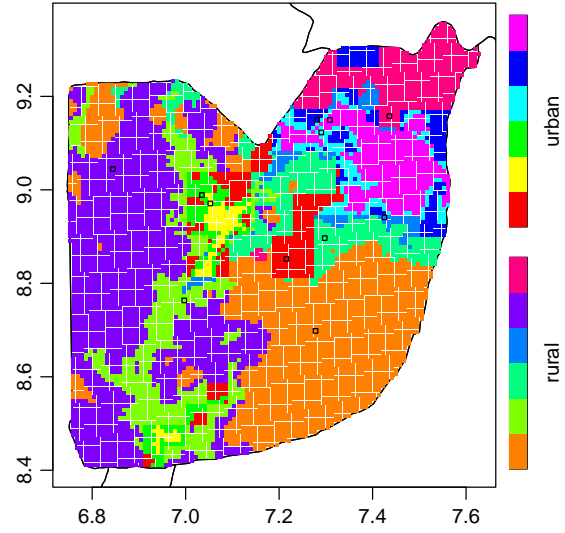


Figure A.3: MICS integration points plotted as black squares surrounding associated fine grid points with nonzero population. Fine grid points are colored by associated integration points (top left), normalized $\log(1 + \text{population})$ (top right), urban/rural classifications (middle left), normalized distance to rivers and lakes (middle right), normalized $\log(1 + \text{healthcare inaccessibility})$ (bottom left), and normalized $\sqrt{\text{elevation}}$ (bottom right) for $K = 25$ integration points in urban and rural parts of FCT Abuja.

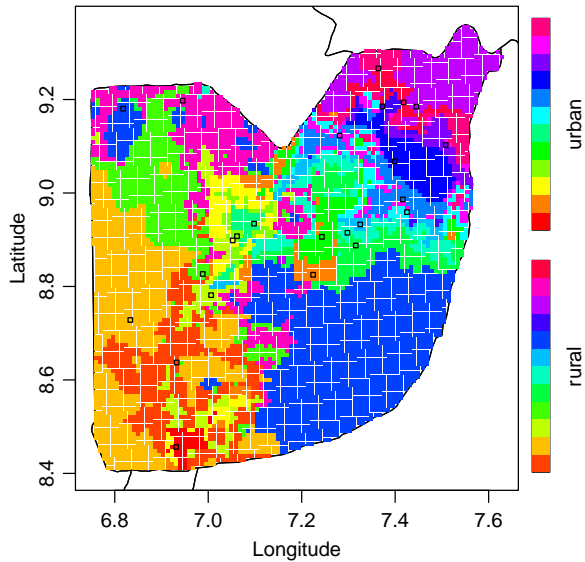
Integration points and associated locations ($K^{\text{MICS}} = 3$)



Integration points and associated locations ($K^{\text{MICS}} = 6$)



Integration points and associated locations ($K^{\text{MICS}} = 12$)



Integration points and associated locations ($K^{\text{MICS}} = 24$)

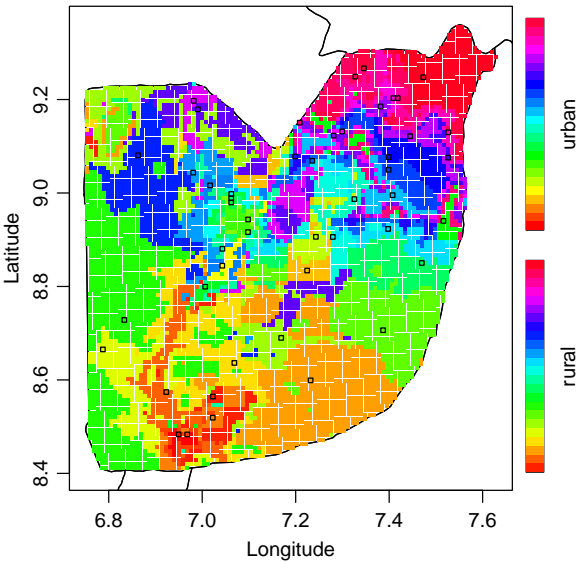


Figure A.4: Integration points plotted as black squares surrounding associated fine grid points colored by associated integration point for $K = 3, 6, 12,$ and 24 for FCT Abuja.

Approach	Bias	RMSE	CRPS	IS	Cvg	Width	Runtime (minutes)
<i>DHS+MICS</i>							
M _d	-0.013	0.240	0.123	0.937	0.93	0.766	0.03
M _D	-0.011	0.240	0.124	0.931	0.93	0.759	1.16
M _{dm}	-0.004	0.244	0.125	0.897	0.94	0.811	0.07
M _{DM}	-0.004	0.243	0.125	0.921	0.93	0.782	13.05
<i>DHS</i>							
M _d	-0.006	0.216	0.112	0.874	0.94	0.742	0.03
M _D	-0.002	0.216	0.112	0.865	0.94	0.739	1.05
M _{dm}	0.001	0.224	0.116	0.862	0.95	0.799	0.07
M _{DM}	0.004	0.225	0.117	0.868	0.94	0.768	13.89
<i>MICS</i>							
M _d	-0.020	0.269	0.137	1.013	0.92	0.794	0.04
M _D	-0.023	0.269	0.137	1.009	0.92	0.783	1.28
M _{dm}	-0.010	0.268	0.135	0.939	0.94	0.826	0.07
M _{DM}	-0.012	0.265	0.134	0.985	0.93	0.800	12.05

Table C.5: Full set of cluster level validation results.

Model	Bias	RMSE	CRPS	IS	Cvg	Width	Runtime (minutes)
<i>DHS+MICS</i>							
M _d	-0.022	0.060	0.042	0.427	0.89	0.236	0.04
M _D	-0.019	0.052	0.037	0.332	0.89	0.222	1.16
M _{dm}	-0.014	0.053	0.040	0.430	0.81	0.208	0.08
M _{DM}	-0.011	0.053	0.039	0.415	0.81	0.203	13.42
<i>DHS</i>							
M _d	-0.016	0.063	0.045	0.554	0.92	0.280	0.04
M _D	-0.013	0.055	0.040	0.478	0.92	0.268	1.16
M _{dm}	-0.009	0.065	0.047	0.520	0.89	0.255	0.08
M _{DM}	-0.005	0.064	0.046	0.519	0.95	0.251	13.42
<i>MICS</i>							
M _d	-0.026	0.074	0.051	0.413	0.95	0.294	0.04
M _D	-0.024	0.068	0.048	0.404	0.92	0.283	1.16
M _{dm}	-0.019	0.067	0.048	0.432	0.89	0.270	0.08
M _{DM}	-0.015	0.067	0.047	0.403	0.89	0.266	13.42

Table C.6: Full set of Admin1 level (areal) validation results.

S.4. Additional results for the application

	Est	Q0.025	Q0.1	Q0.9	Q0.975
(Int)	-1.44	-1.60	-1.55	-1.34	-1.29
urb	1.09	0.91	0.97	1.21	1.27
access	-0.06	-0.13	-0.11	-0.01	0.02
elev	0.12	0.05	0.08	0.17	0.20
distRiversLakes	0.05	-0.03	0.00	0.10	0.13
popValsNorm	0.50	0.36	0.41	0.59	0.63
sigmaSq	0.41	0.24	0.29	0.54	0.62
phi	0.51	0.31	0.39	0.65	0.71
sigmaEpsSq	1.85	1.68	1.73	1.97	2.05

Table D.7: Proposed model posterior parameter central estimates and 95% credible intervals for the M_{dm} model. Covariates are transformed and normalized as described in Section 2.2.

References

- [1] Schubert, E. and Rousseeuw, P. J. (2019). Faster k-medoids clustering: improving the PAM, CLARA, and CLARANS algorithms. In *Similarity Search and Applications: 12th International Conference, SISAP 2019, Newark, NJ, USA, October 2–4, 2019, Proceedings 12*, pages 171–187. Springer.